Transformation of optical speckles by atomic vapors: From Rayleigh to Weibull intensity statistics

I. L. Rodrigues [1,2] J. P. Lopez [1] and T. Passerat de Silans [1,*]

[1]*Departamento de Física, CCEN, Universidade Federal da Paraíba, Caixa Postal 5008, 58051-900 João Pessoa, Paraíba, Brazil*

[2]*Departamento de Física/IFM Universidade Federal da Pelotas, Pelotas, Rio Grande do Sul, Brazil*

(Received 21 December 2023; accepted 12 August 2024; published 26 August 2024)

We investigate the transformation of Rayleigh speckle patterns by an atomic cesium vapor. After propagation through the atomic vapor, the incident exponentially decaying intensity distribution of the Rayleigh speckles is transformed with enhancement of high intensities probabilities (extreme events). The measured intensity distributions are fitted by Weibull distributions. The nonlinear interaction between the atomic vapor and the optical field leads to intensity-dependent refraction and absorption, resulting in changes of the speckle spots' intensities with propagation. We measure the inverse of the shape parameter of the Weibull distributions as a function of laser detuning and interpret the results by modeling the speckle propagation.

DOI: 10.1103/PhysRevA.110.023525

I. INTRODUCTION

When a coherent wave is scattered, a random distribution of intensities is observed, known as a speckle pattern. This pattern is the result of interference of multiple partial waves with a given phase distribution. If the multiple partial waves that interfere have (i) random and independent amplitudes and (ii) random and independent phases uniformly distributed over 2π, the speckle follows a Rayleigh distribution. Rayleigh distribution is characterized by Gaussian distribution of the field's amplitude and a decaying exponential intensity distribution [1].

The investigation of control of speckle patterns for obtaining non-Rayleigh optical speckles has been motivated by numerous applications. For instance, super-Rayleigh speckles were used to reduce signal-to-noise ratio in reconstructed images of ghost imaging [2] due to increase of the patterns' contrast [3] and non-Rayleigh speckle patterns have been used for sub-Rayleigh resolution in images [4,5]. Also, non-Rayleigh speckle patterns can be used to manipulate cold atoms [6] and super-Rayleigh speckles can be used as prototype for studying the formation of rogue waves [7,8].

Non-Rayleigh speckles can be obtained by misleading of one of the conditions for Rayleigh patterns, for instance, by generating partial waves with correlated phase [9–12]. Also, both sub-Rayleigh and super-Rayleigh patterns have been obtained after transmission of Rayleigh patterns by nonlinear media [13,14], for which the refractive index depends on the local intensity $n = n_0 + n_2 I$. Super-Rayleigh patterns have been obtained for positive, focusing, Kerr nonlinearity ($n_2 I > 0$), resulting in heavy-tailed intensity distributions, that is, with increased probability of the occurrence of high-intensity spots (extreme events). For some sets of parameters, intensity distributions become a power law $P(I) \propto I^{\gamma}$ with exponents around $\gamma = -1.5$ [13,14].

Here we investigate the transformation of speckle patterns by a resonant cesium vapor [14]. We show that obtained intensity distributions of the speckle patterns can be fitted with Weibull distributions [15–17]. We develop a theoretical approach that qualitatively reproduces the experimental results and is consistent with the transformation from Rayleigh to Weibull intensity distribution.

II. EXPERIMENT

A. The setup

The experimental setup is shown in Fig. 1 and is similar to the one used in Ref. [14]. We use a tapered amplified diode laser emitting around ∼100-mW at wavelength of cesium D_2 line ($\lambda = 852$ nm). The laser frequency can be finely tuned around the $6S_{1/2}(F = 4) \rightarrow 6P_{3/2}(F' = 3, 4, 5)$ transitions and the laser frequency is monitored by an auxiliary Fabry-Perot interferometer and a saturated-absorption experiment. The beam, with a diameter of 2 mm, passes through a diffuser (with 1° diffusing angle) generating a speckle pattern that will interact with cesium vapor placed 5 cm past the diffuser. The beam power incident on the diffuser is controlled by changing the driving current of the tapered amplifier. The vapor cell has a diameter of 2.5 cm and is 2 cm long. Two independent ovens control the temperature of the vapor and of a sidearm cesium reservoir, with the cesium reservoir allowing one to set the vapor density in the probing volume. After the cell, a lens images the speckle at the cell output window on a CCD camera. The lens is placed at a distance of $2f$ from the cell and from the camera, with $f = 10$ cm, the focal length of the lens, forming an image with no magnification. Before the CCD camera, neutral density filters are used to attenuate the light intensity. The eight-bit CCD camera has pixels of size $2.2\,\mu\text{m} \times 2.2\,\mu\text{m}$ and adjustable exposure time.

*Contact author: thierry@otica.ufpb.br

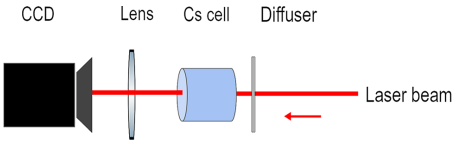

FIG. 1. Scheme of the experimental setup: a laser beam is incident on a commercial diffuser to produce a Rayleigh speckle pattern. The speckle interacts with a cesium vapor and the output speckle pattern is imaged with a CCD camera.

We collect images for different combinations of atomic vapor density, beam power, and frequency detuning. The beam hits the diffuser with a little displacement relative to the diffuser center. For each parameter set, we take ten images by rotating the diffuser to have different realizations of the speckle patterns.

B. Experimental results

We show in Fig. 2 some examples of the speckle patterns obtained by changing the laser detuning and keeping fixed the atomic density and the beam power. Figure 2(a) is for the laser far detuned from resonance ($\delta = 3000$ MHz, we define the detuning δ relative to the $F = 4 \rightarrow F' = 5$ transition); the laser is not interacting with the vapor and the observed pattern is a Rayleigh speckle produced by the diffuser. The intensity probability density function (PDF) of the Rayleigh pattern is a decreasing exponential [1]:

$$P_R(I) = \frac{1}{\bar{I}} e^{-I/\bar{I}}, \tag{1}$$

with $\bar{I}$ being the mean intensity. As the laser frequency is tuned closer to resonance [see Figs. 2(b)–2(d)], the speckle patterns are modified. Laser is blue detuned from the $6S_{1/2}(F = 4) \rightarrow 6P_{3/2}(F' = 5)$ transition for which $n_2 > 0$ corresponding to the autofocusing interaction [18]. Intensity spots become more concentrated and brighter. Intensity PDFs

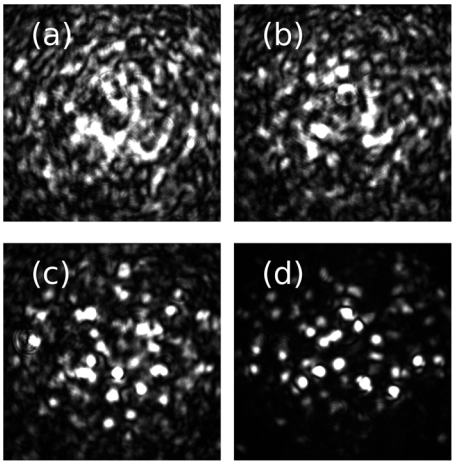

FIG. 2. Examples of speckle patterns past the vapor for an atomic density of $N = 4\times10^{18}$ m^{-3} and a beam power of 90 mW before the diffuser (a) for $\delta = 3000$ MHz, (b) for $\delta = 700$ MHz, (c) for $\delta = 500$ MHz, and (d) for $\delta = 300$ MHz. The size of the images is of 600 pixels×600 pixels.

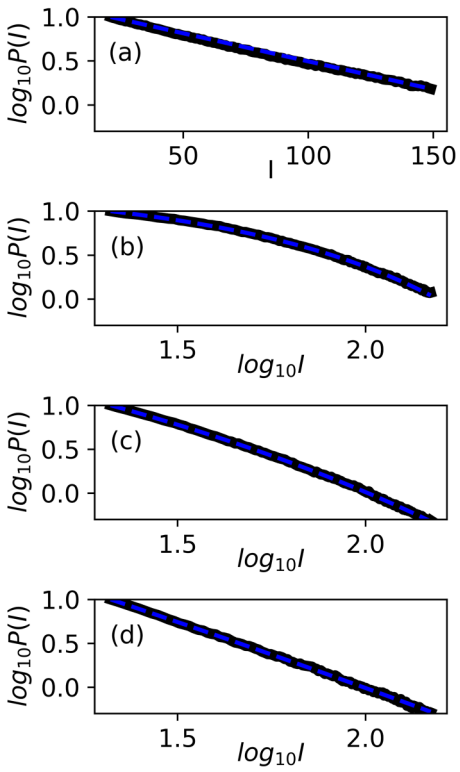

FIG. 3. Probability density function of speckle patterns shown in Fig. 2. The speckle patterns were observed for a density of $N = 4\times10^{18}$ m^{-3} and a beam power of 90 mW before the diffuser and for different laser detunings. (a) $\delta = 3000$ MHz, (b) $\delta = 700$ MHz, (c) $\delta = 500$ MHz, and (d) $\delta = 300$ MHz. Blue dashed lines correspond to fits of experimental data by Weibull distributions of Eq. (2).

corresponding to the speckle patterns shown in Fig. 2 are shown in Fig. 3. The experimental intensity PDFs are fitted by Weibull distributions [15–17]:

$$P_W(I) = \frac{1}{\alpha K \bar{I}} I^{\frac{1-\alpha}{\alpha}} \exp\left[-\frac{I^{1/\alpha}}{K\bar{I}}\right], \tag{2}$$

with α known as the inverse shape parameter.

The Rayleigh distribution is transformed into a Weibull distribution through transformation of the intensity parameter [17]:

$$I = f_{\mathrm{NL}}(I_0) = (KI_0)^{\alpha}, \tag{3}$$

with I being the detected intensity, I_0 the incident intensity and K a parameter to ensure the homogeneity of the transformation:

$$P_W(I) = P\left[f_{\mathrm{NL}}^{-1}(I)\right]\left|\frac{dI_0}{dI}\right|, \tag{4}$$

resulting in the Weibull distribution of Eq. (2).

The Weibull distribution is equal to the Rayleigh distribution for $\alpha = 1$ and resembles a power law for large α and limited dynamical range of observed intensities. For all the sets of parameters used in the experiment, the intensity PDFs were well fitted by Weibull distributions of Eq. (2). The inverse shape parameter α values obtained from fitting the

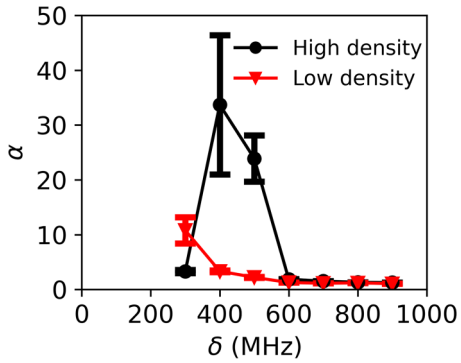

FIG. 4. Obtained inverse shape parameter α by fitting intensity PDFs by Weibull distributions of Eq. (2) as a function of incident laser beam frequency detuning. Black circles denote high density ($N = 8\times10^{18}$ m^{-3}), and red triangles denote low density ($N = 4\times10^{18}$ m^{-3}).

Weibull distributions as a function of laser detuning for two different atomic vapor densities are shown in Fig. 4.

Far from resonance, the beam does not interact with the vapor, and the Rayleigh distribution is observed corresponding to $\alpha \approx 1$. As the laser detuning gets closer to resonance, the Kerr nonlinearity of refractive index increases, strengthening the focusing character of the interaction. As a result, the α parameter increases, reaching values as large as $\alpha \sim 30$. For such α values the experimental intensity PDF approaches a power law with an exponent ~ -1.5 [see, for instance, Fig. 3(d)] as was observed in simulations by Alves *et al.* [14]. For large α, the power law part of the Weibull distribution of Eq. (2) has low sensitivity to the α value and $I^{(1-\alpha)/\alpha} \sim I^{-1}$. The remaining decay of the intensity PDF is given by the exponential part of the Weibull distribution, which can be adjusted by changing simultaneously K and α parameters, resulting in a large variety of parameters pairs (α, K) with the correct decay of the intensity PDF and large error bars for high α values. For still smaller detuning, $\delta \sim 300$ MHz, linear absorption depletes the pattern intensity, lowering the nonlinear contribution of the refractive index and lowering the α fitted value.

Abscissa axes of Fig. 3 are given in level of intensity (ranging from 0 to 255 for our eight-bit CCD). We have calibrated the camera and an intensity level equal to 1 corresponds to an intensity after the sample of $I = 20$ mW/cm^2 $\sim 12.5 I_S$, with I_S being the saturation intensity of the vapor that we define in Sec. III B. Thus, the detected range of intensities is $\sim 250 I_S$ to $\sim 1875 I_S$.

III. DISCUSSION

The atomic vapor acts as a nonlinear medium transforming the input Rayleigh intensity distribution. For the intensity distribution of the transformed pattern to be consistent with a Weibull distribution, a power law relation between input intensity and output intensity must occur [see Eq. (3)].

We model the transformation function $f_{\rm NL}(I)$, related both to focusing of the speckle pattern by positive Kerr nonlinearity and to absorption by the vapor, and verify if it is consistent with Eq. (3).

A. Model of $f_{\rm NL}$

To model the transformation function $f_{\rm NL}$ we consider each speckle spot evolving independently of the others. Each spot is modeled as a Gaussian beam with an aberration-free propagation; that is, the beam remains Gaussian during propagation and the index of the refraction gradient is assumed to be parabolic [19–21]. For a thin sample, the parabolic shape of the refractive index results in the medium acting as a spherical lens. A thick sample can in turn be modeled by an array of spherical lenses [20] with focal distances:

$$f_m = \frac{w_m^2}{4 n_m^{(\rm NL)} \Delta L}, \tag{5}$$

with f_m being the focal length of the mth lens in the array, w_m the beam waist, and $n_m^{(\rm NL)}$ the nonlinear part of the refractive index at the mth lens position. $\Delta L = L/M$ is the distance between consecutive lenses, with L being the sample thickness and M the number of lenses modeled.

The evolution of the speckle spot is calculated using the ABCD matrix formalism by the change on the Gaussian q parameter [22]:

$$q_m = \frac{A_{m-1} q_{m-1} + B_{m-1}}{C_{m-1} q_{m-1} + D_{m-1}}, \tag{6}$$

with

$$\begin{pmatrix} A_{m-1} & B_{m-1} \\ C_{m-1} & D_{m-1} \end{pmatrix} = \begin{pmatrix} 1 - \frac{\Delta L}{f_{m-1}} & \Delta L \\ -1/f_{m-1} & 1 \end{pmatrix}. \tag{7}$$

Equations (6) and (7) describe the transformation of the Gaussian q parameter after passing through a lens of focal length f_m and propagating a distance ΔL in free space [20]. The Gaussian q parameter is related to the radius of curvature of the wave front R and to the beam radius w at position z as [22]

$$\frac{1}{q(z)} = \frac{1}{R(z)} - i \frac{\lambda}{\pi n w^2(z)}. \tag{8}$$

At each lens position, the intensity is calculated as

$$I_m = \frac{2 P_m}{\pi w_m^2}, \tag{9}$$

where P_m is the beam spot power and the waist is extracted from $w_m^2 = \frac{\lambda}{\pi}[\mathrm{Im}(1/q_m)]^{-1}$. To take into account absorption by the vapor, the power is attenuated by $P_m = P_{m-1}[1 - \beta(I_m)\Delta L]$, with $\beta(I)$ being the intensity-dependent absorption coefficient. As the beam arrives collimated on the diffuser (infinite radius of curvature), we take initial q parameter as $q_0 = i\frac{\pi w_0^2}{\lambda}$, with w_0 being the spot size at the cell entrance.

B. Calculations of the nonlinear refractive index and the absorption coefficient

To calculate the optical properties of the atomic vapor that influence the Gaussian spot propagation we consider an ensemble of two-level atoms with inhomogeneous Doppler broadening. The two-level model is justified because we analyze frequencies blue detuned ($\delta > 0$) relative to the cycling transition $6S_{1/2}(F = 4) \rightarrow 6P_{3/2}(F' = 5)$ that dominates the transitions to excited hyperfine manyfold with a relative

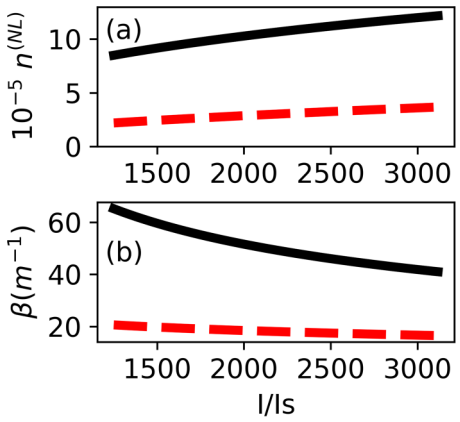

FIG. 5. Calculated (a) $n^{(\mathrm{NL})}(I)$ and (b) $\beta(I)$ for $\delta = 300\,\mathrm{MHz}$ (black solid line) and $\delta = 500\,\mathrm{MHz}$ (red dashed line) for a density of $N = 2\times10^{18}\ \mathrm{m}^{-3}$.

strength of 11/18 [23]. The two-level atom is a saturable system with optical susceptibility [24]:

$$\chi(\delta, I) = \int dv \frac{1}{u\sqrt{\pi}} e^{-v^2/u^2} \chi(\delta, I, v), \tag{10}$$

with $\chi(\delta, I, v)$ being the velocity-dependent susceptibility [24]:

$$\chi(\delta, I, v) = N\mu^2 \frac{4}{\epsilon_0 \hbar \Gamma^2} \frac{(\delta - kv) - i\Gamma/2}{1 + \frac{4(\delta - kv)^2}{\Gamma^2} + \frac{I}{I_S}}, \tag{11}$$

with the saturation intensity given by $I_S = \frac{\epsilon_0 c \hbar^2 \Gamma^2}{4\mu^2}$. Here u is the most probable speed of the Maxwell-Boltzmann distribution, Γ is the excited level decay rate, μ is the electric dipole moment of the transition, N is the atomic density, and ϵ_0 is the vacuum permittivity.

The intensity-dependent absorption coefficient is given by $\beta(I) = \frac{2\pi}{\lambda}\mathrm{Im}[\chi(\delta, I)]$ and the intensity-dependent refractive index is $n = 1 + \frac{1}{2}\mathrm{Re}[\chi(\delta, I)]$. We calculate the nonlinear contribution of the refractive index as

$$n^{(\mathrm{NL})}(\delta, I) = n(\delta, I) - n(\delta, 0), \tag{12}$$

which can be taken as an effective Kerr nonlinearity $n^{(\mathrm{NL})} = n_2^{\mathrm{eff}} I$ [25,26].

We plot in Fig. 5 the calculated $n^{(\mathrm{NL})}(\delta, I)$ and $\beta(\delta, I)$ for a range of intensities and detunings similar to those used in the experiment. In the high-intensity regime, such that power broadening is larger than Doppler broadening ($\Gamma\sqrt{(1 + I/I_S)} > \Gamma_D = \frac{u}{\lambda}$), $n^{(\mathrm{NL})}(\delta, I)$ and $\beta(\delta, I)$ can be approximated by [27]

$$n^{(\mathrm{NL})}(\delta, I) \approx [1 - n(\delta, I = 0)] \frac{I/I_S}{1 + 4\delta^2/\Gamma^2 + I/I_S} \tag{13}$$

and

$$\beta(\delta, I) \propto \frac{1}{1 + 4\delta^2/[\Gamma^2(1 + I/I_S)]} \frac{1}{1 + I/I_S}. \tag{14}$$

On the one hand, the smaller the detuning is, the higher $n^{(\mathrm{NL})}$ [see Fig. 5(a)] and the lens effect are. On the other hand, having smaller detuning implies stronger depletion of intensity by absorption [see Fig. 5(b)].

TABLE I. Optical properties of D_2 transition of cesium atoms and parameters used in model calculations: μ is the electric dipole moment, Γ is the excited level decay rate, Γ_D is the Doppler width for a vapor temperature of 130 °C, L is the cell thickness, M is the number of lenses used in the model, w_0 is the incident beam waist, and I_0 is the incident intensity for calculations of Figs. 6 and 7.

Cesium D_2 transition optical properties			
μ	Γ	Γ_D	I_S
2.19 C m	$2\pi\times5.23$ MHz	$2\pi\times260$ MHz	1.65 W/m^2
Parameters used in calculations			
L	M	w_0	I_0
2 cm	2000	40 μm	$2500 I_S$

C. Evolution of the beam along the vapor and the Weibull inverse shape parameter α

Using the model described in Secs. III A and III B, we calculate the output intensity I, past the sample, as a function of the input intensity I_0 for different detunings and atomic densities. As we model the output intensity by Eq. (3), we extract the Weibull parameter from $\alpha = \frac{d\ln(I)}{d\ln(I_0)}$. Parameters used in the calculations as well as optical properties of the cesium D_2 line are given in Table I.

We plot in Fig. 6(a) the evolution of the beam waist as a function of the position inside the sample for low atomic density. First, we impose $n^{(\mathrm{NL})} = 0$ in our calculations (blue dotted line with $\delta = 300\,\mathrm{MHz}$); that is, the waist increases only due to beam diffraction. As a result, the intensity decreases along the propagation [see blue dotted line in Fig. 6(b)]. For large detuning [$\delta = 500\,\mathrm{MHz}$, see red-dash-dotted lines in Figs. 6(a) and 6(b)], the nonlinear refractive index is not high and the evolution of the beam waist and the beam intensity almost follows a linear regime. Moreover, in this case, due to high intensity ($I \gg I_S$), intensity depletion due to absorption is low and plays a little role. The transformation function f_{NL} is thus almost linear with intensity, resulting in $\alpha \approx 1$ [see Eq. (3)]. For smaller detuning ($\delta = 300\,\mathrm{MHz}$), the nonlinear refractive index lens effect (autofocusing) acts

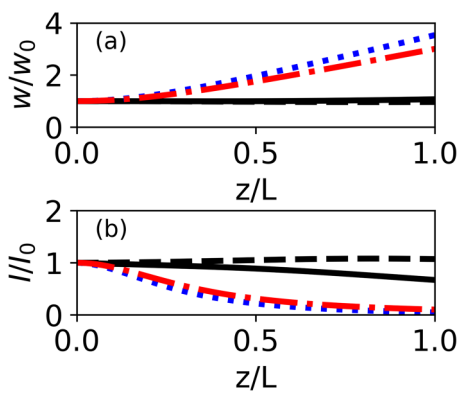

FIG. 6. Calculated evolution of the beam (a) waist and (b) intensity during propagation along the sample. Calculations were done for low density ($N = 0.8\times10^{18}\ \mathrm{m}^{-3}$). Black solid line, $\delta = 300$ MHz; black dashed line, $\delta = 300\,\mathrm{MHz}$ and $\beta = 0$; blue dotted line, $\delta = 300\,\mathrm{MHz}$ and $n^{(\mathrm{NL})} = 0$; and red dash-dotted line, $\delta = 500\,\mathrm{MHz}$.

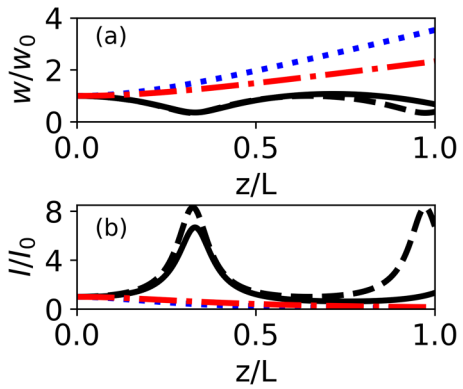

FIG. 7. Calculated evolution of the beam (a) waist and (b) intensity during propagation along the sample. Calculations were done for high density ($N = 2\times10^{18}$ m^{-3}). Black solid line, $\delta = 300$ MHz; black dashed line $\delta = 300$ MHz and $\beta = 0$; blue dotted line, $\delta = 300$ MHz and $n^{(\mathrm{NL})} = 0$; red dash-dotted line, $\delta = 500$ MHz.

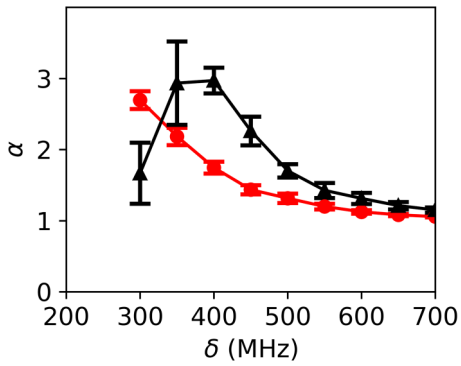

FIG. 8. Calculated Weibull parameter α as a function of detuning for low (red circles) and high (black triangles) densities, respectively, $N = 0.8\times10^{18}$ m^{-3} and $N = 2\times10^{18}$ m^{-3}.

and beam diffraction is balanced by focusing, resulting in an almost constant waist [see black solid line in Fig. 6(a)]. The intensity, thus, remains almost constant, slightly decreasing due to absorption [see the black solid line in Fig. 6(b) and compare with the black dashed line which shows the calculations for null absorption $\beta = 0$]. As $n^{(\mathrm{NL})}$ increases and $\beta(I)$ decreases with the input intensity (see Fig. 5), the output intensity I is sensitive to the input, resulting in $\alpha > 1$.

The same evolution of the beam waist and intensity is calculated for the higher density (see Fig. 7), for which we expect larger effects since $n^{(\mathrm{NL})}$ and β are proportional to the density. For $\delta = 500$ MHz (red dash-dotted line), autofocusing counterbalance diffraction and a Weibull parameter $\alpha > 1$ are expected. For $\delta = 300$ MHz [see black solid lines in Figs. 7(a) and 7(b)], one observes a strong decrease of the waist due to high $n^{(\mathrm{NL})}$ value. After reaching a minimum waist value, linear diffraction overcomes nonlinear focusing and the waist increases until focusing overcomes diffraction again and the waist decreases again. The waist evolves in an oscillation mode [19]. Absorption delays the waist oscillations and, eventually, eliminates them by depleting the energy and thus decreasing $n^{(\mathrm{NL})}$ (please, compare with the black dashed line, for which we have imposed $\beta = 0$). In the case where autofocusing is strong and the beam waist oscillates, the obtained Weibull α parameter depends on which part of the oscillation the waist is at the end of the sample.

To verify if our model is consistent with the proposed transformation of Eq. (3), the calculated parameter $\alpha = \frac{d\ln(I)}{d\ln(I_0)}$ must be almost constant over a given intensity range. The input intensity range used is such that it results in the measured range of the output intensity (see Fig. 3 and discussion in Sec. II B), which is set by the camera setting parameters (basically the exposure time) and optical attenuating elements. The obtained α values for low and high densities are shown in Fig. 8, with each point and error bar being the mean and standard deviation of calculated α values for the chosen input intensity range.

For low density, the smaller the detuning is, the higher $n^{(\mathrm{NL})}$ and the focusing effect are. The focusing effect counterbalances the diffraction of the beam, lowering the beam waist and increasing the intensity. As the input intensity is much higher than the saturating intensity, the saturated absorption coefficient [Eq. (14)] is low and absorption has minor effect on energy depletion (compare the black solid line and the black dashed line in Fig. 6). Also, the saturated nonlinear refractive index [see Eq. (13)] is almost independent of the intensity, resulting in low standard deviation of the estimated α value.

For high density, $n^{(\mathrm{NL})}$ is sufficiently high at moderate detuning $\delta \sim 400$–500 MHz to counterbalance diffraction, resulting in a high α value. For low detuning, the depletion of energy by absorption renders oscillations of the beam waist longer or even eliminates them. The calculated α value then depends on where the oscillation has stopped and, thus, on the input intensity, resulting in large error bar values ($\sim\frac{\sigma_\alpha}{\alpha} \approx 0.25$, with σ_α being the standard deviation of obtained α). If absorption is high enough, the depletion of energy diminishes the nonlinear refraction, lowering the inverse shape parameter α as observed for $\delta = 300$ MHz and high density (see Figs. 4 and 8).

In the calculations of the evolution of the beam along the sample we have used a parameter value of $w_0 = 40$ μm, which corresponds approximately to the waist of the Gaussian beam resulting from the diffuser divergence angle of 1°. The atomic densities used theoretically have given the better results in qualitative comparison with experiments and are lower than those estimated for the experiment. The use of lower densities in the theoretical analysis has the effect of smoothing the nonlinear focusing effects and is justified since it is expected that the nonlinear focusing effect is lower under experimental conditions relative to the model used sincefor the following reasons.

(i) We consider an aberration free theory (parabolic refractive index); however, a real beam has aberrations which lower the rate of growth of intensity in the beam axis, smoothing the nonlinear effect as the beam propagates [19].

(ii) The Kerr self-focusing effect is smoothed for non-Gaussian beams. In Ref. [28], it was shown that the Rayleigh range of the Hermite-Gauss mode propagating in Kerr media increases with the mode order along with a reduction of the focusing effect. Thus, nonfundamental HG modes in the decomposition of non-Gaussian beams contribute to smoothing of nonlinear focusing.

(iii) Saturation of the Kerr coefficient broadens the refractive index profile and makes it more flat around the beam center [29,30], smoothing the lens effect.

IV. CONCLUSIONS

In conclusion, we have obtained non-Rayleigh speckle patterns after interaction of Rayleigh speckles with an atomic vapor. The nonlinear interaction of the optical field with the vapor results in a positive nonlinear refractive index (focusing). The autofocusing of the speckle spots increases the high intensity values, enhancing the probability of finding extreme values [13,14]. The obtained intensity PDFs of the transmitted speckle patterns are well fitted by Weibull distributions with an inverse shape parameter α greater than 1. For some experimental set of parameters, values of the inverse shape parameter as large as $\alpha \sim 30$ are obtained, for which intensity PDFs approach a power law [13,14] for finite dynamical range.

We have modeled the system as independent spots propagating in the vapor under the action of positive refraction nonlinearity and absorption. The Weibull distribution is obtained under a transformation of the input intensity to the transmitted intensity of the form $I \propto I_0^{\alpha}$ [17] due to decrease of the spot waist by autofocusing. For low detuning and high atomic density, the depletion of energy might diminish the focusing effect, resulting in a detuning and density dependence of the inverse shape parameter that is well reproduced by the model. Although we obtain, both in experiment and theory, a large incertitude of α for intensity PDFs with high-α parameters, we assume the Weibull distribution is the correct one. The argument for this is that Weibull distributions fit well all curves for all sets of experimental parameters, indicating the same physics. Speckle transformation was previously modeled by propagation of solitons in Kerr medium [31] resulting in an output intensity distribution written as the product of a power law decay and an exponential decay, as is the case in Weibull distribution (however, not with the same relation between the exponents of the power law and the exponential argument). The control of the transmitted speckle patterns might impact a variety of applications, for instance, the study of rogue wave formation [7,8] and the manipulation of particles [6].

ACKNOWLEDGMENTS

The authors acknowledge financial support from Coordenação de Aperfeiçomento de Pessoal de Nível Superior (CAPES), Conselho Nacional de Desenvolvimento Científico e Tecnológico (CNPq, Grant No. 405180/2021-7) and Fundação de Apoio à Pesquisa do Estado da Paraíba (FAPESQ, Grant No. 2021/3218). This work was funded by the Public Call No. 03 Produtividade em Pesquisa PROPESQ/PRPG/UFPB, Grant No. PVA13235-2020.

[1] J. W. Goodman, *Speckle Phenomena in Optics: Theory and Applications*, Press Monographs (SPIE Press, Bellingham, Washington, 2020).

[2] S. Liu, Z. Liu, C. Hu, E. Li, X. Shen, and S. Han, Spectral ghost imaging camera with super-Rayleigh modulator, Opt. Commun. **472**, 126017 (2020).

[3] W. Gong and S. Han, A method to improve the visibility of ghost images obtained by thermal light, Phys. Lett. A **374**, 1005 (2010).

[4] S. Zhang, W. Wang, R. Yu, and X. Yang, High-order correlation of non-Rayleigh speckle fields and its application in super-resolution imaging, Laser Phys. **26**, 055007 (2016).

[5] Z. Li, X. Nie, F. Yang, X. Liu, D. Liu, X. Dong, X. Zhao, T. Peng, M. S. Zubairy, and M. O. Scully, Sub-Rayleigh second-order correlation imaging using spatially distributive colored noise speckle patterns, Opt. Express **29**, 19621 (2021).

[6] D. Delande and G. Orso, Mobility edge for cold atoms in laser speckle potentials, Phys. Rev. Lett. **113**, 060601 (2014).

[7] A. Mathis, L. Froehly, S. Toenger, F. Dias, G. Genty, and J. M. Dudley, Caustic and rogue waves in an optical sea, Sci. Rep. **5**, 12822 (2015).

[8] S. Choudhary, A. N. Black, A. Antikainen, and R. W. Boyd, Controlling nonlinear rogue-wave formation using the coherence length of phase noise, Phys. Rev. Res. **6**, 013174 (2024).

[9] Y. Bromberg and H. Cao, Generating non-Rayleigh speckles with tailored intensity statistics, Phys. Rev. Lett. **112**, 213904 (2014).

[10] X. Li, Y. Tay, H. Li, J. Wang, H. Wang, and Z. Nie, Generation of a super-Rayleigh speckle field via a spatial light modulator, Appl. Phys. B **122**, 82 (2016).

[11] N. Bender, H. Yilmaz, Y. Bromberg, and H. Cao, Customizing speckle intensity statistics, Optica **5**, 595 (2018).

[12] N. Bender, H. Yılmaz, Y. Bromberg, and H. Cao, Creating and controlling complex light, APL Photon. **4**, 110806 (2019).

[13] Y. Bromberg, Y. Lahini, E. Small, and Y. Silberberg, Hanbury Brown and Twiss interferometry with interacting photons, Nat. Photon. **4**, 721 (2010).

[14] S. B. Alves, H. L. D. de S. Cavalcante, G. F. de Oliveira, Jr., T. P. de Silans, I. Vidal, M. Chevrollier, and M. Oriá, Controlling the intensity statistics of speckle patterns: From normal to subthermal or superthermal distributions, Phys. Rev. A **99**, 033838 (2019).

[15] W. Weibull, A statistical distribution function of wide applicability, J. Appl. Mech. **18**, 293 (1951).

[16] R. Barrios and F. Dios, Exponentiated Weibull distribution family under aperture averaging for Gaussian beam waves, Opt. Express **20**, 13055 (2012).

[17] J. P. Amaral, E. J. S. Fonseca, and A. J. Jesus-Silva, Tailoring speckles with Weibull intensity statistics, Phys. Rev. A **92**, 063851 (2015).

[18] M. O. Araújo, H. L. D. de S. Cavalcante, M. Oriá, M. Chevrollier, T. P. de Silans, R. Castro, and D. Moretti, Measurement of the Kerr nonlinear refractive index of Cs vapor, Phys. Rev. A **88**, 063818 (2013).

[19] S. A. Akhmanov, A. P. Sukhorukov, and R. V. Khokhlov, Self-focusing and diffraction of light in a nonlinear medium, Sov. Phys. Usp. **10**, 609 (1968).

[20] M. Sheik-Bahae, A. Said, D. Hagan, M. Soileau, and E. Vanstryland, Nonlinear refraction and optical limiting in thick media, Opt. Eng. **30**, 1228 (1991).

[21] V. Magni, G. Cerullo, and S. De Silvestri, ABCD matrix analysis of propagation of Gaussian beams through Kerr media, Opt. Commun. **96**, 348 (1993).

[22] H. Kogelnik and T. Li, Laser beams and resonators, Appl. Opt. **5**, 1550 (1966).

[23] D. Steck, Cesium d line data, http://steck.us/alkalidata, 2019.

[24] R. W. Boyd, *Nonlinear Optics*, 2nd ed. (Academic Press, San Diego, 2003).

[25] A. S. Reyna and C. B. de Araújo, Nonlinearity management of photonic composites and observation of spatial-modulation instability due to quintic nonlinearity, Phys. Rev. A **89**, 063803 (2014).

[26] F. C. D. dos Santos, J. C. de Aquino Carvalho, G. T. Moura, and T. P. de Silans, Measurement of the nonlinear refractive index of Cs D_1 line using Z-scan, J. Opt. Soc. Am. B **36**, 2468 (2019).

[27] D. H. Close, Strong-field saturation effects in laser media, Phys. Rev. **153**, 360 (1967).

[28] X. Fan, X. Ji, H. Yu, H. Wang, Y. Deng, and L. Chen, Kerr effect on propagation characteristics of Hermite-Gaussian beams, Opt. Express **27**, 23112 (2019).

[29] B. Gu and H.-T. Wang, Theoretical study of saturable Kerr nonlinearity using top-hat beam Z-scan technique, Opt. Commun. **263**, 322 (2006).

[30] J. F. dos Santos, G. G. Costa, D. N. Messias, and T. Catunda, Theoretical study of high order and saturable Kerr media nonlinearities in Z-scan, Opt. Commun. **479**, 126421 (2021).

[31] S. Derevyanko and E. Small, Nonlinear propagation of an optical speckle field, Phys. Rev. A **85**, 053816 (2012).